CHEMISTRY
A European Journal

A Journal of
ChemPubSoc Europe

Accepted Article

Title: Quadruple Stimuli-Responsive Mechanized Silica Nanoparticles: A Promising Multifunctional Nanomaterial for Diverse Applications

Authors: Chendi Ding, Ling Tong, and JiaJun Fu

To be cited as: *Chem. Eur. J.* 10.1002/chem.201704245

Link to VoR: http://dx.doi.org/10.1002/chem.201704245

Supported by
ACES

WILEY-VCH

10.1002/chem.201704245

WILEY-VCH

Quadruple Stimuli-Responsive Mechanized Silica Nanoparticles: A Promising Multifunctional Nanomaterial for Diverse Applications

ChenDi Ding,[a] Ling Tong[a] and JiaJun Fu*[a]

Abstract: Novel quadruple stimuli-responsive mechanized silica nanoparticles were constructed by installation of supramolecular nanovalves onto exterior surface of mesoporous silica nanoparticles. The release of cargo molecules is triggered by acid/Zn^{2+}/alkali/reduction potential stimuli, which offers application prospects of developing the drug delivery systems or construction of smart anticorrosion coatings.

Stimuli-responsive controlled release systems, which are capable of executing predefined missions of on-demand cargo release through chemical or physical changes in configurations upon external stimuli, have received considerable attentions.[1] Inorganic or polymeric materials, acting as nanocarriers, are decorated by various gatekeepers, including nanoparticles, polymer, proteins, DNA, and supramolecular architectures, which provide the ideal templates for synthesizing stimuli-responsive controlled release systems.[2] Recently, with the development and deepening of research for supramolecular host-guest chemistry, the elaborately designed rotaxanes/pseudorotaxanes as supramolecular nanovalves have been immobilized on the exterior surface of mesoporous silica nanoparticles (MSNs) and regulated the diffusion in or out of the cargo molecules, which is depending on the stimuli-induced mechanical movement of macrocyclic molecules along synthetic linear molecular stalks.[3] Based on these assembly conception, a vast of mechanized silica nanoparticles (MSNPs) have emerged in the last decade and showed the great potential in the field of drug delivery systems due to the inherent ability of making the timely feedback to endogenous stimuli surrounding tumor issues (pH,[4] redox,[5] enzyme[6] *etc*.) or exogenous stimuli (light,[7] thermo[8] *etc*.) and delivering anticancer drugs to targeted tumor sites. Compared with single or dual stimuli-responsive systems, multiple stimuli-responsive MSNPs not only provide the possibility of precisely controlling the dosage and location for cargo molecules *via* rational arrangement of the multi-stimuli,[9] but also achieve more functions, which will undoubtedly expand their potential application fields by integrating appropriate stimuli into one controlled release system. Also, the more kinds of stimulus that controlled release systems could recognize, the smarter it would be for multiple application fields.Therefore, recently more and more researchers place an emphasis in developing multiple stimuli-responsive MSNPs.

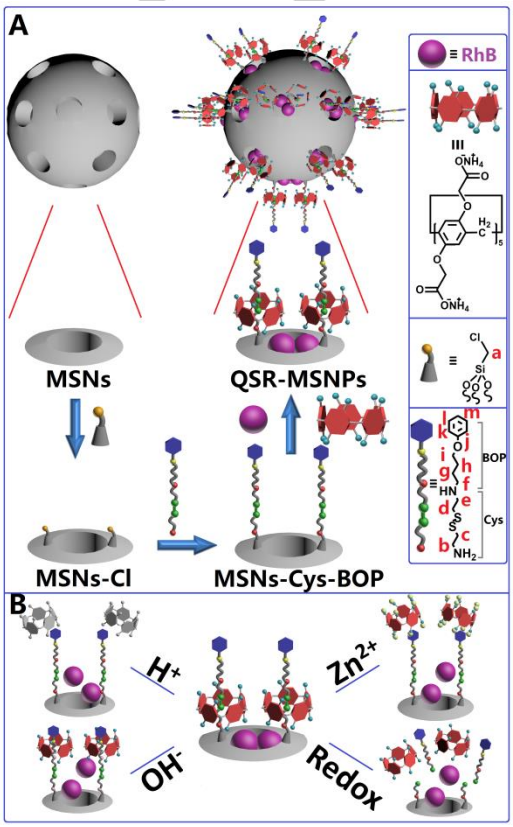

Scheme 1. Schematic illustration of (A) fabrication of QSR-MSNPs; (B) stimuli-responsive release mechanism of QSR-MSNPs.

Herein, we tailored the acid/Zn^{2+}/alkali/reduction potential quadruple-stimuli responsive MSNPs (QSR-MSNPs) for the first time to achieve multiple application purpose, where the MSNs were employed to accommodate cargo molecules and the crucial components were [2]pseudorotaxanes, composed of water soluble pillar[5]arene (WP[5], see Supporting Information for details, Figure S1 and S2) and 2,2'-dithiobis(ethanamine)-N-butoxybenzene (Cys-BOP, see Supporting Information for details, Figure S3-S10). In neutral solution, WP[5] bind with the first recognizable motif, cystamine (Cys) in linear functional stalks, preventing the undesirable leakage of cargo molecules. The working mechanism of QSR-MSNPs is schematically depicted in Scheme 1B. The four different controlled release approaches are explained as following: (i) alkali stimulus drives WP[5] to transfer from Cys motif to the second recognizable motif, N-butoxybenzene (BOP), leaving entrances for cargo molecules; (ii) acidic stimulus facilitates the precipitation of WP[5] from QSR-MSNPs and the gatekeepers are lost. (iii) the addition of Zn^{2+} generates the competitive binding interactions, which spurs Zn^{2+}-WP[5] complexes to dissociate from the linear

[a] Dr. C. Ding, L. Tong, Prof. J. Fu
School of Chemical Engineering
Nanjing University of Science and Technology
Nanjing 210094 (P.R. China)
E-mail: fujiajun668@gmail.com

Supporting information for this article is given via a link at the end of the document.

10.1002/chem.201704245

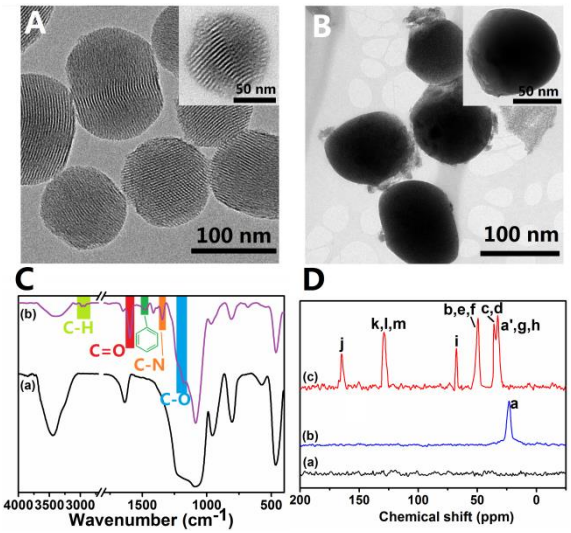

Figure 1. TEM image of (A) MSNs; (B) QSR-MSNPs; (C) FTIR spectra of MSNs, (b) QSR-MSNPs; (D) ^{13}C SS-NMR spectra of (a) MSNs, (b) MSNs-Cl, (c) MSNs-Cys-BOP.

functional stalks; (vi) after exerting reduction potential, the disulfide bonds in Cys motif are broken, resulting in the disintegration of supramolecular nanovalves.

The typical MCM-41 type, mono-dispersed MSNs with the average diameter of about 105 nm are shown in the transmission electron microscopy (TEM) image (Figure. 1A). The high-ordered hexagonal mesoporous structure was confirmed by TEM image and small-angle X-ray diffraction (SA-XRD) data (Figure S11). N_2 absorption-desorption isotherm of MSN exhibited a type IV isotherm with a high specific surface area of 1135.4 m^2 g^{-1}, a large total pore volume of 0.89 cm^3 g^{-1}, and the narrow pore diameter of 2.38 nm (Figure S12). The synthetic route for QSR-MSNPs is illustrated in Scheme 1A. The surface of MSNs was successively functionalized with chloromethyltriethoxysilane (CMTES) and Cys-BOP to afford MSNs-Cl and MSNs-Cys-BOP, respectively. The whole functionalization process was characterized by fourier transform infrared spectroscopy (FTIR) and ^{13}C solid-state nuclear magnetic resonance (^{13}C SS-NMR). As shown in Figure.1D (b), the resonance signal at 22.9 ppm was assigned to methylene group of MSNs-Cl; and the typical absorption peaks of C-H asymmetrical stretching vibration (2856 and 2958 cm^{-1}) and C-Cl stretching vibration (690 cm^{-1}) in the FTIR spectrum (Figure S13(a)) also suggested that CMTES anchored on the surface of MSNs. For MSNs-Cys-BOP, FTIR result showed new absorption bands at 1546, 1513 and 1383 cm^{-1}, which are respectively assigned to the characteristic absorption peak of shear vibration of N-H, skeleton vibration of benzene ring and C-N stretching vibration, indicating the covalent conjugation of Cys-BOP (Figure S13(b)). Furthermore, the ^{13}C SS-NMR spectrum of MSNs-Cys-BOP (Figure.1D (c)) displays two series of signals: (i) $C_{a'}$, C_g, and C_h (29.2-33.8 ppm), C_c and C_d (35-37.3 ppm), C_b, C_e and C_f (46.4-54.2 ppm) are all belonging to the aliphatic moieties; (ii) C_i (67.9 ppm), C_k, C_l and C_m (125.6-131.2 ppm), and C_j (165.3 ppm) are corresponding to the phenol moieties. The uniform distributions of C, N and S within the MSNs-CysBOP, exhibited in energy dispersive X-ray analysis (EDAX) mapping images, also suggest the full coverage of the intact functionalized stalks on the surface exterior (Figure S14). After loading rhodamine (RhB, Figure S13(c)) and undergoing the self-assembly process between WP[5] and Cys-BOP, QSR-MSNPs were successfully constructed. The FTIR spectrum of QSR-MSNPs exhibits the characteristic peak of C=O stretching vibration at 1600 cm^{-1} and C-O asymmetrical stretching vibration at 1175 cm^{-1}, proving the incorporation of WP[5] and RhB. In addition, as the assembly process proceeded step-by-step, XRD peak intensities gradually decreased and the texture parameters dramatically declined concurrently (Figure S15, S16 and Table S1) due to the partial occupation of pore volume by functional stalks and RhB. The TEM image for QSR-MSNPs illustrates the uniform coverage of supramolecular nanovalves on surface of MSNs (Figure. 1B). According to the results from thermogravimetric analysis (TGA), the contents of grafted CMTES and CysBOP were determined as 0.86 mmol g^{-1} and 0.43 mmol g^{-1}, respectively, as well as the weight loss of RhB and WP[5] was roughly estimated as 13.1% (Figure S17).

Release experiments were carried out under different types of stimuli in PBS (pH 7.4). The loading of RhB was calculated to be 173.3 μmol g^{-1} QSR-MSNPs (Figure S18). Prior to application of triggers, the flat baseline within 24 h shown in Figure. 2A demonstrated the negligible leakage of RhB, meaning the closed pore orifices. The complexation between WP[5] and Cys-BOP was investigated by ^1H NMR spectroscopy. The addition of 1.0 equiv. of WP[5] to a solution of Cys-BOP in D_2O resulted in the remarkable upfield chemical shifts of the Cys protons, H_h ($\Delta\delta_h$=-1.1 ppm), H_i ($\Delta\delta_i$=-3.1 ppm), H_j ($\Delta\delta_j$=-2.8 ppm), and H_k ($\Delta\delta_k$=-1.0 ppm) due to the shielding effect of the electron-rich cavities of WP[5], while no obvious change was observed for the BOP protons (Figure. 2C (d and e)). Further isothermal titration calorimetry (ITC) measurement indicated that WP[5] could form a stable 1:1 binding stoichiometry with an association constant of 1.21×10^6 M^{-1} (Figure S19). Under neutral solution, WP[5] resided on the Cys motif steadily, near the pore orifices. [2]pseudorotaxane **1a** sealed the entrances for diffusion out of RhB. Upon addition of HCl, the substantial RhB was released, and the cumulative release efficiency was 9.09 % at pH=6.0 and increased to 69.95% at pH=2.0 after 24 h. As shown in Figure. 2C (f). Adding DCl into WP[5]⊃CysBOP caused the disappearance of protons of WP[5] and the slight shifting of partial Cys-BOP protons was ascribed to the protonation of -NH- and -NH_2 groups. Based on these results, it is understandable that the protonation of carboxylate groups on both ends of WP[5] leads to the precipitation of WP[5] (Figure S20), which equates to open the supramolecular nanovalves and frees RhB. The phenomenon of alkali-stimuli responsive release was also observed (Figure. 2B). With the addition of NaOD, the Cys protons returned back to their original locations, whereas the protons in BOP motif strongly shielded ($\Delta\delta_{c,d,g,e,f}$=-0.2, -1.7, -1.6, -1.0, and -1.1 ppm, Figure. 2C (a and b)). Obviously, alkali stimulus drives WP[5] mechanically move from Cys motif to BOP motif. The ITC data also substantiate this migration process. The association constant between WP[5] and Cys motif is controlled by pH of solution, which decreased from 4.96×10^5 M^{-1} (neutral) to 1.62×10^4 M^{-1} (alkali) (Figure S21). In contrast, the association

10.1002/chem.201704245

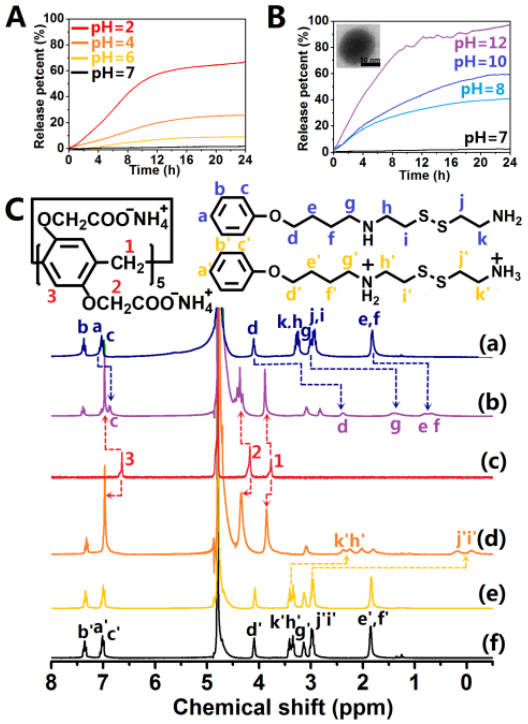

Figure 2. (A) Acid-triggered release profiles of RhB; (B) alkali-triggered release profiles of RhB, insert image: TEM image of QSR-MSNPs after the release experiment in alkaline environment; (C) ^{1}H NMR spectra (300 MHz, D_2O, 298K): (a) 5mM Cys-BOP, pD=10.0; (b) 5mM Cys-BOP and 5mM WP[5], pD=10.0; (c) 5 mM WP[5]; (d) 5 mM Cys-BOP and 5 mM WP[5], pD = 7.0; (e) 5 mM Cys-BOP, pD = 7.0; (f) 5 mM Cys-BOP and 5 mM WP[5], pD = 2.0.

constant between WP[5] and BOP motif (see Supporting Information for synthetic procedure, Figure S22-S25) was stable and calculated as 1.39×10^{5} M^{-1} (Figure S21). For QSR-MSNPs, WP[5] encircled on the BOP motif, signifying that the gatekeepers are far away from the pore orifices. [2]pseudorotaxane **1b** works as opened switch, realizing the release of RhB from the mesopores. Noticeably, TEM photo (Figure S26) shows that the morphology of QSR-MSNPs after release experiment remained stable, which excludes the possibility that such release behavior is caused by disassembly of scaffold material in alkaline environment. The control experiments were also conducted to certify the blocking role of WP[5] (Figure S27).

There have been some reports concerning that divalent metal ions has the ability to damage the structures of WP[6]-based supramolecular assemblies.[10,11] In this study, in the presence of Zn^{2+}, QSR-MSNPs showed excellent performance of controlled release. The release efficiency of RhB from QSR-MSNPs was observed to increase with the increase of Zn^{2+} concentration. After completing release experiment, the Zn^{2+}-WP[5] complexes were detected in the supernatant (Figure S28), which demonstrates the chelation of Zn^{2+} between carboxylate groups on WP[5] destroy the WP[5]⊃CysBOP, making WP[5] dissociate from the functional stalks and accomplishing the release task. The natural discrepancy in Zinc concentration between normal issues and central nervous system disease sites[12] inspires us to develop Zn^{2+}-triggered controlled release systems, and thus achieve active targeted drug delivery. Astoundingly, when reduction potential (-1.0 V vs SHE) was exerted, RhB was rapidly released and by exerting oxidative potential (+1.0 vs

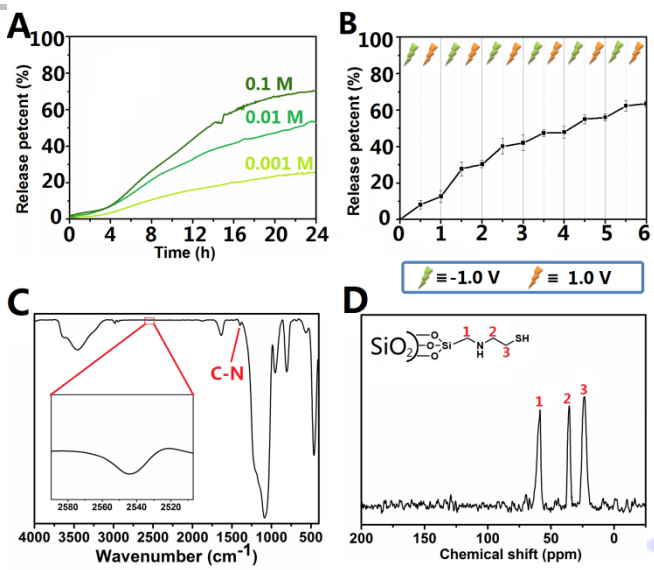

Figure 3. (A) Zn^{2+}-triggered release profiles of RhB; (B) Reductive/oxidative potential-triggered release profiles of RhB; (C) FTIR spectrum of QSR-MSNPs treated with -1.0 V potential. (Insert: expanded spectrum) (D) ^{13}C SS-NMR spectrum of QSR-MSNPs treated with -1.0 V potential.

SHE), the release trend of RhB was greatly inhibited. This is due to that the disulfide could be re-formed under oxidative environment[13] and therefore the blocking effect of supramolecular switches was partially recovered. The potential sensitivity is associated with the disulfide bonds in Cys motif, which is evidenced by the FTIR and ^{13}C SS-NMR spectra (Figure 3C and 3D) of residue solids collected after receiving reduction potential stimulus: The absorption peak at 1380 cm^{-1} represents the C-N stretching vibration, at the same time, a weak absorption peak appeared at 2545 cm^{-1}, which confirms the existence of thiol groups. Combined with results of ^{13}C SS-NMR, the organic components immobilized on surface of MSNs is inferred as methylcysteamine, testifying that the generating electrons entered into cavity of WP[5] and subsequently cleave the disulfide bonds, completely undermining the supramolecular nanovalves. It is worth noting that glutathione (GSH) did not initiate the release of RhB from QSR-MSNPs (Figure S29). Calculation results indicated that due to the size effect, GSH cannot entered into the cavity of WP[5], originally complexed with Cys, and have no opportunity to contact with disulfide bonds (Figure S30).

Taking advantage of slightly acidic environments in cancerous tissues, endosomes and lysosomes as compared to physiological pH in the blood and normal tissues, QSR-MSNPs have the potential to deliver anticancer drugs to the tumor sites. In order to evaluate QSR-MSNPs as qualified nanovehicles, MTT assay was conducted against MCF-7 cancer cells and NIH3T3 normal cells in the presence of various concentrations of empty QSR-MSNPs, doxorubicin (DOX)-loaded QSR-MSNPs and free DOX. As model anticancer drug for substitution of RhB, DOX was loaded into QSR-MSNPs, (the encapsulation efficiency is 121.4 μmol g^{-1}, Figure S31) which also exhibited the acid stimulus-responsive release characteristic, while under neutral condition, even with the addition of 10% serum, DOX barely released (Figure. 4A). As shown in Figure. 4B and Figure. S32, after incubation for 24 h, empty QSR-MSNPs were nontoxic to MCF-7 and NIH3T3 normal cells at all the tested concentration, revealing their excellent biocompatibility. In

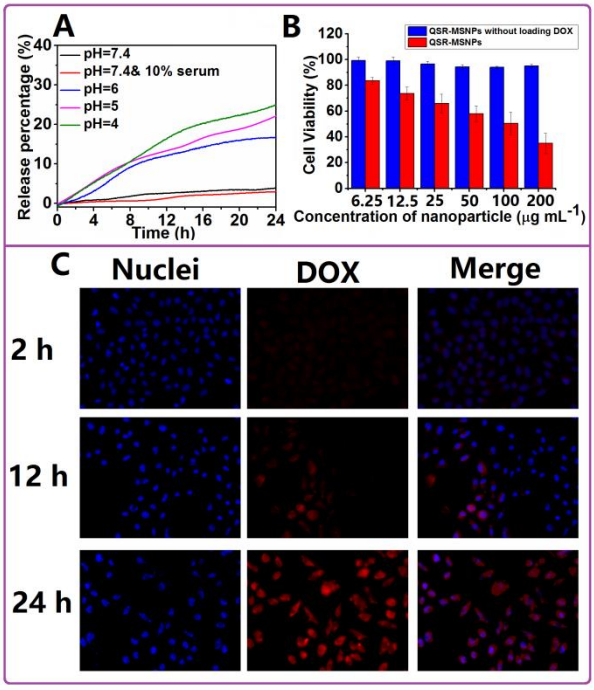

Figure 4. (A) Acid-triggered release profiles of DOX from QSR-MSNPs; (B) Cytotoxicity of empty QSR-MSNPs, DOX-loaded QSR-MSNPs, and free DOX after 24 h of cell culture using MCF-7 cells; (C) Fluorescent images of MCF-7 cells incubated with QSR-MSNPs (12.5 μg mL^{-1}) for different incubation time, from left to right: Hoechst 33342 (blue), DOX (red) and a merged images.

contrast, significant growth inhibition on MCF-7 cancer cells was observed when incubated either with DOX-loaded QSR-MSNPs or free DOX (Figure S33). The cytotoxicity presented clear dosage-dependency (the IC50 was calculated to be which is 126.3 μg/mL and the corresponding DOX amount is 8.3 μg/mL) and the cell viability remarkably decreased as the increase of the effective DOX concentration. For comparison, DOX-loaded QSR-MSNPs manifested the slightly lower inhibition activity than those treated with the free DOX at the equivalent dosage. The representative fluorescence merged images shown in Figure. 4C depicts the three stages for transport process of DOX: (i) DOX was confined within QSR-MSNPs and almost no DOX red fluorescence was observed due to the quenching effects. (ii) QSR-MSNPs were taken up by cancer cells and acid-triggered intracellular release of DOX occurred. Noticeably, DOX was primarily located in the cell cytoplasm at this stage. (iii) DOX eventually diffused into nuclei and showed the killing effect toward MCF-7 cells.

Another potential application of QSR-MSNPs is to construct smart anticorrosion coatings for protection of aluminum alloys, which often suffers from local corrosion due to its poor corrosion resistance. Once the aggressive species (Cl-, O_2 etc.) penetrate through protective coatings and reach aluminum alloy surface, the local corrosion will be initiated, which leads to the environmental changes in the local regions: (i) in the corrosive micro-anodic regions, the dissolution of metallic Al and hydrolysis of Al^{3+} causes local acidification; (ii) in the corrosive micro-cathodic regions, the oxygen reduction reaction results in the local alkalization[14]; (iii) electrons transferring from anodic to cathodic regions bring about the decrease in surface electrochemical potential15 (for AA2024, -1.05 V vs. SHE). QSR-MSNPs possessing acid/alkali/reduction potential stimuli-responsiveness guarantees that no matter where QSR-MSNPs

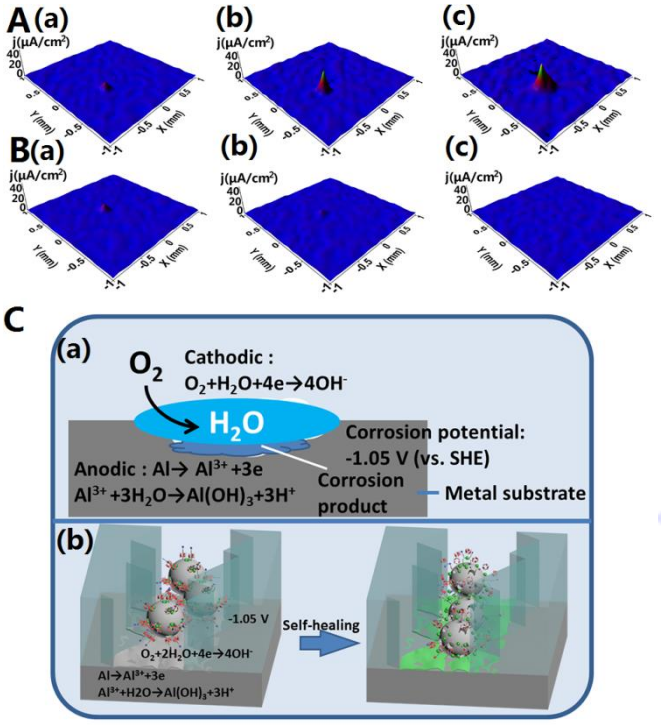

Figure 5. (A) SVET results of (A) the control coating sample, (B) QSR-MSNPs loaded coating sample for immersion in 0.5 M NaCl of (a) 5 h, (b) 12 h, (c) 24 h. (C) Schematic illustration of (a) corrosion of AA2024; (b) working mechanism of QSR-MSNPs in smart anticorrosion coatings.

are located (micro-anodic, cathodic regions or regions between them), they can rapidly respond to these three stimuli and immediately give the feedback to release corrosion inhibitors to restrict corrosion propagation. To testify the above concept, benzotriazole (BTA) was employed as corrosion inhibitor and loaded into QSR-MSNPs (loading amount: 142.7 μmol g^{-1}, Figure S34). As shown in Figure S35, the release of BTA triggered by acid/alkali/reduction potential stimuli was also observed. QSR-MSNPs as nanocontainers were doped into sol-gel coating (Figure S36) and the self-healing performances of hybrid coating was evaluated by scanning vibrating electrode technique (SVET). As shown in Figure 5, the corrosion current density of hybrid coating around artificial defects decreased rapidly over time, while for the control coating (so-gel coating without QSR-MSNPs), the current density kept growing to 37.95 μA cm^{-2} at the end of monitoring. SEM images and EDAX mapping (Figure S37) for artificial defects verify the role of QSR-MSNPs in the self-healing process. The timely release of BTA and subsequent formation of BTA molecular film on local damaged region account for the effect suppression of local corrosive activity. (Figure 5C).

In summary, the quadruple stimuli-responsive mechanized silica nanoparticles were successfully prepared, in which the supramolecular nanovalves installed onto the exterior surface of MSNs implement the switch behaviors and control the release of cargoes. The unique controlled release properties expand their application fields. QSR-MSNPs are expected to be used in the field of targeted drug delivery systems to avoid side effects due to their acid/Zn^{2+} stimuli-responsiveness. Meanwhile, acid/alkali/reduction potential stimuli-responsive controlled release characteristic enhances the response sensitivity of QSR-MSNPs as nanocontainers in smart anticorrosion coatings, and thus improves self-healing effects.

Acknowledgements

This research was financially supported by the National Nature Science Foundation of China (No. 51672133), the Natural Science Foundation of Jiangsu Province (No. BK20161496), the fundamental Research Funds for the Central Universities (No. 30915012207), Postgraduate Research & Practice Innovation Program of Jiangsu Province (No. KYCX17_0374) and a project funded by the Priority Academic Program Development of Jiangsu Higher Education Institutions (PAPD). Authors ChenDi Ding and Ling Tong contributed equally to this work.

Keywords: host–guest chemistry • supramolecular nanovalves • stimuli-responsive • controlled release • mesoporous nanoparticles

[1] a) Y. Cong, Q. Li, M. Chen, L. Wu, *Angew. Chem. Int. Ed.* **2017**, *56*, 3552-3556; b) Y. Wang, M. S. Shim, N. S. Levinson, H. W. Sung, Y. Xia, *Adv. Funct. Mater.* **2014**, *24*, 4206-4220.

[2] a) S. Wu, X. Huang, X. Du, *J. Mater. Chem. B* **2015**, *3*, 1426-1432; b) N. Barooah, A. Kunwar, R. Khurana, A. C. Bhasikuttan, J. Mohanty, *Chem. - Asian J.* **2017**, *12*, 122-129; c) D. Xiao, H. Z. Jia, J. Zhang, C. W. Liu, R. X. Zhuo, X. Z. Zhang, *Small* **2014**, *10*, 591-598; d) C. H. Lu, I. Willner, *Angew. Chem. Int. Ed.* **2015**, *54*, 12212-12235; e) A. A. Hwang, J. Lu, F. Tamanoi, J. I. Zink, *Small* **2015**, *11*, 319-328; f) N. Song, Y. W. Yang, *Chem. Soc. Rev.* **2015**, *44*, 3474-3504; g) Y. L. Sun, Y. W. Yang, D. X. Chen, G. Wang, Y. Zhou, C. Y. Wang J. F. Stoddart, *Small* **2013**, *19*, 3224-3229.

[3] a) Y. W. Yang, Y. L. Sun, N. Song, *Acc. Chem. Res.* **2014**, *47*, 1950-1960; b) X. Ma, Y. Zhao, *Chem. Rev.* **2014**, *115*, 7794-7839; c) M. W. Ambrogio, C. R. Thomas, Y. L. Zhao, J. I. Zink, J. F. Stoddart, *Acc. Chem. Res.* **2011**, *44*, 903-913; d) E. Aznar, M. Oroval, L. Pascual, J. R. Murguía, R. Martínez-Máñez, F. Sancenón, *Chem. Rev.* **2016**, *116*, 561-718; e) S. Alberti, G. J. A. A. Soler-Illia, O. Azzaroni, *Chem. Commun.* **2015**, *51*, 6050-6075.

[4] a) Q. L. Li, Y. Sun, Y. L. Sun, J. Wen, Y. Zhou, Q. M. Bing, L. D. Isaacs, Y. Jin, H. Gao, Y. W. Yang, *Chem. Mater.* **2014**, *26*, 6418-6431; b) T. Wang, M. Wang, C. Ding, J. Fu, *Chem. Commun.* **2014**, *50*, 12469-12472; c) T. Chen, N. Yang, J. Fu, *Chem. Commun.* **2013**, *49*, 6555-6557; d) Z. Li, D. L. Clemens, B. Y. Lee, B. J. Dillon, M. A. Horwitz, J. I. Zink, *ACS nano* **2015**, *9*, 10778-10789.

[5] a) Z. Luo, X. Ding, Y. Hu, S. Wu, Y. Xiang, Y. Zeng, B. Zhang, H. Yan, H. Zhang, L. Zhu, *ACS nano* **2013**, *7*, 10271-10284; b) Q. L. Li, S. H. Xu, H. Zhou, X. Wang, B. Dong, H. Gao, J. Tang, Y. W. Yang, *ACS Appl. Mater. Interfaces* **2015**, *7*, 28656-28664.

[6] a) M. Xue, J. I. Zink, *J. Am. Chem. Soc.* **2013**, *135*, 17659-17662; b) A. Llopis-Lorente, P. Díez, C. de la Torre, A. Sánchez, F. Sancenón, E. Aznar, M. D. Marcos, P. Martínez-Ruíz, R. Martínez-Máñez, R. Villalonga, *Chem. - Eur. J.* **2017**, *23*, 4276-4281.

[7] a) D. Wang, S. Wu, *Langmuir* **2016**, *32*, 632-636; b) A. Martinez-Cuezva, S. Valero-Moya, M. Alajarin, J. Berna, *Chem. Commun.* **2015**, *51*, 14501-14504; c) H. Li, L. L. Tan, P. Jia, Q. L. Li, Y. L. Sun, J. Zhang Y. Q. Ning, J. Yu, Y. W. Yang, *Chem. Sci.* **2014**, *5*, 2804-2808; d) T. M. Guardado-Alvarez, L. Sudha Devi, M. M. Russell, B. J. Schwartz, J. I. Zink, *J. Am. Chem. Soc.* **2013**, *135*, 14000-14003.

[8] a) X. Wang, L. L. Tan, X. Li, N. Song, Z. Li, J. N. Hu, Y. M. Cheng, Y. Wang, Y. W. Yang, *Chem. Commun.* **2016**, *52*, 13775-13778; b) J. Dong, J. I. Zink, *Small* **2015**, *11*, 4165-4172; c) J. Croissant, J. I. Zink, *J Am. Chem. Soc.* **2012**, *134*, 7628-7631.

[9] a) J. Wei, X. J. Ju, X. Y. Zou, R. Xie, W. Wang, Y. M. Liu, L. Y. Chu, *Adv. Funct. Mater.* **2014**, *24*, 3312-3323; b) X. An, A. Zhu, H. Luo, H. Ke, H. Chen, Y. Zhao, *Acs Nano* **2016**, *10*, 5947-5958.c) Y. Zhou, L. L. Tan, Q. L. Li, X. L. Qiu, A. D. Qi, Y. Tao, Y. W. Yang, *Chem. – Eur. J.* **2014**, *20*, 2998-3004.

[10] X. Huang, X. Du, *ACS Appl. Mater. Interfaces* **2014**, *6*, 20430-20436.

[11] L. L. Tan, H. Li, Y. Zhou, Y. Zhang, X. Feng, B. Wang, Y. W. Yang, *Small* **2015**, *11*, 3807-3813.

[12] C. J. Frederickson, S. W. Suh, D. Silva, C. J. Frederickson, R. B. Thompson, *J. Nutr.* **2000**, *130*, 1471S-1483S.

[13] J. A. Yoon, J. Kamada, K. Koynov, J. Mohin, R. Nicolay, Y. Zhang, A. C. Balazs. Tomasz Kowalewski, K. Matyjaszewski, *Macromolecules* **2012**, *45*, 142-149.

[14] D. Snihirova, S. V. Lamaka. M. Taryba, A. N. Salak, S. Kallip, M. L. Zheludkevich, M. G. S. Ferreira, M. F. Montemor, *Appl. Mater. Interfaces* **2010**, *2*, 3011-3022.

[15] A. Vimalanandan, L. Lv, T.H. Tran, K. Landfester, D. Crespy, M. Rohowerder, *Adv. Mater.* **2013**, *48*, 6980-6984.

10.1002/chem.201704245

WILEY-VCH

Entry for the Table of Contents

COMMUNICATION

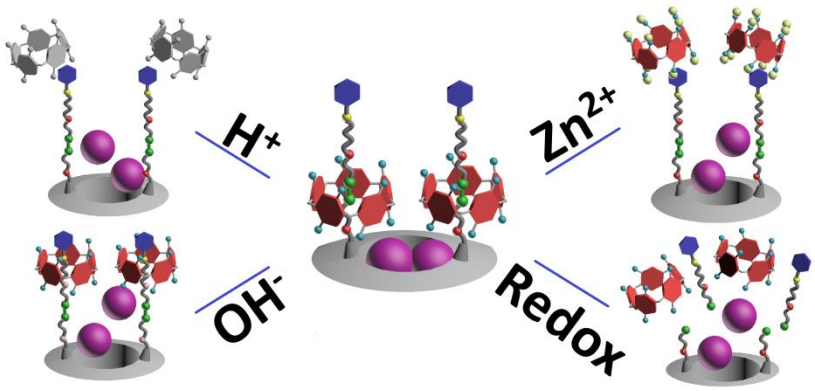

Mesoporous silica nanoparticles grafted with unique supramolecular nanovalves: The controlled release behaviors could be triggered by quadruple stimuli-acid/alkaline/Zn^{2+}/reduction stimuli.

*ChenDi Ding, Ling Tong, JiaJun Fu**

Page No. – Page No.

Quadruple Stimuli-Responsive Mechanized Silica Nanoparticles: A Promising Multifunctional Nanomaterial for Diverse Applications